Adaptive Slicing for Multi-axis Hybrid Plasma Deposition and Milling

Wang Xiangping†, Zhang Haiou†, Wang Guilan*, Wu Lingpeng†

† School of Mechanical Science and Engineering, Huazhong University of Science & Technology, Wuhan 430074, P. R. China
* School of Materials Science and Engineering, Huazhong University of Science & Technology, Wuhan 430074, P. R. China
* wgllab@mail.hust.edu.cn
REVIEWED

Abstract

Hybrid Plasma Deposition and Milling (HPDM), a five-axis manufacturing system integrated material additive and subtractive processes, can be used to create overhang metallic components directly without the usage of sacrificial support structure. Different from conventional slicing methods, a new slicing algorithm with changeable direction and thickness is proposed in this paper. Minimal overhang length is selected as the objective function to optimize the build direction. The thickness is adjusted to meet allowable overhang length and allowable cups height. The input mesh is first decomposed into non-uniform thickness segment meshes and then each segment is cut into uniform thickness slices. The output slices consist of split slices between two adjacent segment meshes and inner slices for each segment mesh. Examples and analyses confirm the feasibility and effectiveness.

Introduction

Additive manufacturing (AM) is a set of digital manufacturing technologies integrated CAD (Computer Aided Design), CAM (Computer Aided Manufacturing) and CNC (Computer Numerical Control). Different from the past, more work is now focused on metal than plastic and various kinds of direct fabrication processes such as SMD (Shaped Metal Deposition), LENS (Laser Engineered Net Shaping) and SLM (Selective Laser Sintering) have been sprung up. In recent years, metallic component direct fabrication without the usage of sacrificial support structure has been one of hot topics in the AM field. However, it is usually necessary to add extra support for building overhang component in the conventional 2.5-axis manufacturing platform. The support will result in the following problems:

1. Design aspect. There is no uniform standard to guide the support design and it is hard to design support for components with high geometry complexity.
2. Fabrication aspect. The material of support is usually different from the material of the component. The manufacturing efficiency will be reduced because of t the material transformation. In addition, it will waste the material and improve cost because the support is sacrificial.
3. The remove of the support is a time-consuming process and the quality of the split surface is poor.

The emergence of multi-axis manufacturing system provides the chance for metallic component direct production without the usage of support. It always keeps the previous built piece as the support of the following building piece by changing the build direction. The component is first decomposed into several sub-volumes and then each sub-volume is created along a fixed direction. Another factor is the effect of surface tension. It makes it possible to fabricate the volume with micro-overhang without the usage of the support.

Therefore, it is urgent to provide a new slicing method to meet the demands of multi-axis manufacturing system. Different the conventional slicing methods, the cruces of multi-axis slicing involve the build direction and the segmentation. Singh [1] and Sundaram [2] used isoclines to decompose the CAD model into two pieces. One is manufacturable and another is hard to make. However, it is necessary to specify the reference build direction and is hard to use for triangular mesh because of discretization error. Similar the visibility map, Singh and Dutta [1] proposed the concept of build map with respect to the overhang angle by using Gauss map. The build map is the set of all feasible build directions. On the basis of the build map, the component is decomposed and the optimal direction is computed in accordance with different targets such as minimal stair-stepping error, minimal volume error and maximal efficiency. However, it is difficult to compute the build map because it refers to complex intersection operations involving the intersection between the half-space and the sphere. Therefore, it is hard to implement. Zhang and Liou [3] defined the overhang angle by using the estimated tangent vector. The build direction is optimized to meet minimal spherical crown which encloses Gauss maps of all sampling tangent vector. The computation is incremental and complex. In addition, it will lead to unexpected results when the sampling tangent vector is few.

Central axis, also known as skeleton, is the 1-dimesion abstract representation for a 1-dimesion object. It has been extensively used for image dissection and retrieval [4-5]. Similar the central axis, the concept of centroid axis [6-8] is proposed and used for overhang part decomposition. The centroid axis is the loci of the centers of all slices and guides the feasible build direction. The advantage is simple and easy to implement. However, the estimating precision is closely related to the slice thickness. It is hard to balance the efficiency and the precision. In addition, the estimating centroid axis will deviate from the actual skeleton when the surface has sharp corner. In this case, it will be failed. Literature [8] provided a improved version by comparing the areas between two adjacent slices and defined several potential slicing directions. It can only figure out the case of orthogonal sharp corner.

HPDM (Hybrid Plasma Deposition Manufacturing) [9-11], a five-axis manufacturing system integrated material additive and subtractive processes, can be used to create overhang metallic components directly without the usage of sacrificial support structure. Fig.1 illustrates the fabrication course of an overhang component. The component is decomposed into five pieces each of which has micro-overhang and can be directly built. The previous piece will turn into the support for the following piece by rotating the A-axis. Therefore, a multi-axis adaptive slicing algorithm is studied to realize overhang component direct fabrication using multi-axis HPDM in

this paper

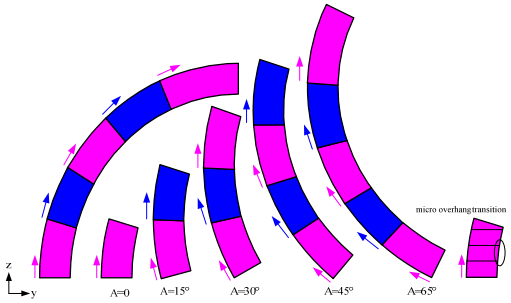

Fig.1 Fabrication of overhang component using multi-axis HPDM

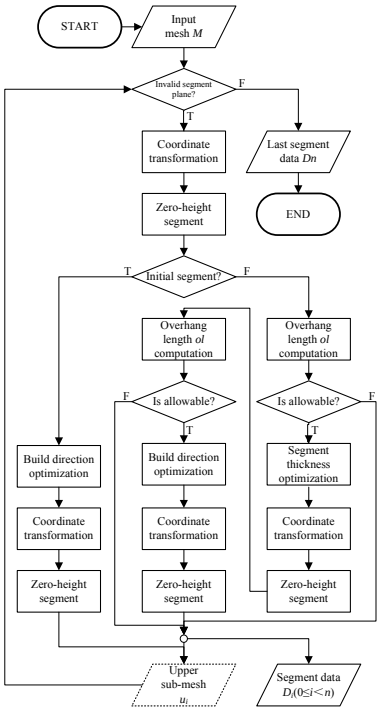

Fig.2 Flow chart of mesh segmentation algorithm

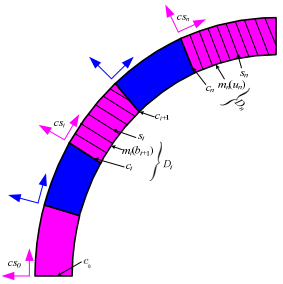

Fig.3 Structure of the segment data

Algorithm overview

The proposed slicing algorithm consists of multi-directional segmentation and single-directional slicing. The former is applied to the input mesh to generate a series of non-uniform segment meshes, each of which can be fabricated directly without the usage of support. The latter is served for each sub-mesh to generate a series of slices, each of which with the same thickness is uniform. Although both of them are implemented by a plane intersection with a mesh, the direction of the plane for the segmentation is changeable and that for the slicing is constant. It is well known that the result of the plane intersection with the mesh is a polygonal contour. To differentiate them, the plane and the contour for the segmentation are called **segment plane** and **segment contour** and they for the slicing are called **slice plane** and **slice contour**.

As shown in Fig.2, given a triangular mesh *M*, the input arguments are listed in Table 1 and the output is a set of segment data (see Fig.3). Each segment data consists of a coordinate system, a segment mesh, a segment under contour and a group of slice contours. The first three items are generated from the segmentation and the last item is generated from the slicing.

The segment plane is determined by the centroid of the trial segment contour and the optimum build direction. To segment the mesh in a unified way, coordinate transformation is first applied to the mesh and then a zero-height segment is carried out. The objective coordinate system takes the optimum build direction as the Z-axis and the centroid as the origin. Zero-height segment decomposes the mesh into two

pieces. One is called **under mesh** with segment plane as the top and another is called **upper mesh** with segment plane as the bottom. The segmentation includes initial segmentation and overhang segmentation. The former generates the initial build direction and the target mesh for overhang segmentation. The latter optimizes the build direction and segment thickness and generates segment plane and segment data. Each segment mesh is formed by two adjacent segmentations. The previous provides the under boundary and the next provides the upper boundary. The under boundary of the first segment mesh is determined by the initial segmentation and the upper boundary of the last segment mesh is determined by the input mesh. Suppose the input mesh is decomposed into n segment meshes. If $0 \leq i < n$, the upper mesh u_i for the ith segmentation is served as the source mesh for the $(i+1)$th segmentation and the under mesh b_{i+1} for the $(i+1)$th segmentation is served as the segment mesh for the ith segmentation. If $i = n$, the segment mesh, namely the last one, is the upper mesh for the nth segmentation.

Table 1 Input arguments/mm

Allowable cusp height	$c_{\max}$	Allowable overhang length	$sol_{\max}$
Maximum segment thickness	$t_{\max}$	Minimum segment thickness	$t_{\min}$
Initial segment height	sh	Slice thickness	st

Overhang measurement between two adjacent layers

Let C_b and C_t denote the projections of two adjacent segment contours L_b and L_t onto the segment plane, called the bottom contour and the top contour respectively. Let A_b and A_t denote the closed regions bounded by C_b and C_t. According to the containment relationship between A and C, we have:

1. If $C_t \subseteq A_b$, there is no overhang between L_b and L_t.
2. If $C_t \nsubseteq A_b$ and $A_b \cap A_t = \emptyset$, there is a large overhang between L_b and L_t.
3. If $C_t \nsubseteq A_b$ and $A_b \cap A_t \neq \emptyset$, there is a small overhang between L_b and L_t.

The large overhang can be converted into the small overhang by the reduction of segment thickness, so the latter is our main research subject. As shown in Fig.4, let V be a point on the top contour C_t. If $V \notin A_b$, it is called an **overhang point** and is denoted by $V \in O$; otherwise, it is called a **non-overhang point** and is written by $V \notin O$. If V is an overhang point, the distance away from the bottom contour C_b is defined as **point-based overhang length** and is formulated by:

$$ol(V, C_b) = dist(V, C_b) \tag{1}$$

Similarly, the distance between C_t and C_b is defined as **contour-based overhang length** represented by the maximum point-based overhang length:

$$ol(C_t, C_b) = \max\{ol(V_1, C_b), ol(V_2, C_b), \cdots, ol(V_k, C_b)\} \tag{2}$$

The recognition of overhang point can be implemented by the intersection between the bottom contour C_b and the ray ray: $\left(P, \overrightarrow{VP}\right)$ where P is a point in the A_b. For a given point $V \in C_t$, we have:

1. If $ray \cap C_b = \emptyset$, $V \notin O$.

2. If $ray \cap C_b \neq \emptyset,\ V \in O$.

For a triangular mesh, the segment contour is a polygon and represented by a set of ordered segments $C := \{s^1, s^2, \cdots, s^n\}$, the intersection and the point-based overhang length can be formulated as:

$$ray \cap C_b = \bigcup_{i=1}^{n} ray \cap s_b^i \tag{3}$$

$$ol(V, C_b) = \min\{dist(V, s_b^1), dist(V, s_b^2), \cdots, dist(V, s_b^n)\} \tag{4}$$

On the basis of the computation of the point-based overhang length, the contour-based overhang length $ol(C_t, C_b)$ can be easily got and served for the recognition of the overhang contour. Therefore, we have:

1. If $ol(C_t, C_b) > 0$, there is a overhang between L_b and L_t.
2. If $ol(C_t, C_b) \leq 0$, there is no overhang between L_b and L_t.

Overhang measurement for a single layer

If there is a overhang between L_b and L_t, the overhang measurement for a single layer L_t now is discussed. As shown in Fig.5, for a given point V_i on the top contour C_t, the overhang angle θ_i is defined as the included angle between the optimum build direction $\boldsymbol{b_i}$ and the actual build direction $\boldsymbol{u}$ and is formulated by:

$$\cos\theta_i = \langle \boldsymbol{b_i}, \boldsymbol{u} \rangle \tag{5}$$

Let t denote the segment thickness, there is a relationship between the overhang angle and the overhang length:

$$ol_i \approx t \cdot \tan(\theta_i) \tag{6}$$

For a segment contour C, we define the summation of all point-based overhang lengths as the contour-based overhang length:

$$ol(C) = \sum_{i=1}^{k} ol_i \tag{7}$$

Given a build direction, the optimum build direction with respect to the point V_i can be estimated by its tangent vector:

$$\boldsymbol{b_i} = \boldsymbol{n_i} \times \boldsymbol{u} \times \boldsymbol{n_i} \tag{8}$$

where $\boldsymbol{n_i}$ denotes the normal vector with respect to the point V_i.

For a triangular mesh, the normal vector $\boldsymbol{n_i}$ can be estimated by the mean of the facet normal vectors:

$$n = \frac{\sum_{i=1}^{k} \boldsymbol{f_i}}{\| \sum_{i=1}^{k} \boldsymbol{f_i} \|} \tag{9}$$

where f_i denote an adjacent facet of V_i. If V_i is the vertex of a facet, k is the valence of the vertex; otherwise, V_i must be the intersection between the segment plane and an edge and $k \doteq 2$

Build direction optimization

The build direction minimizing the overhang length $ol(C)$ is the optimum direction for the upper mesh. If an overhang point V_i can be fabricated directly, its overhang angle must meet $\theta_i \in [0, \pi/2)$ according to the concept of the visible map [12]. When $\boldsymbol{b_i}$ and $\boldsymbol{b}$ are unit vectors, we first translate them onto a Gauss sphere (see Fig.6) and then have:

$$ol_i \propto l_i \propto {}^{1}/_{m_i} \tag{10}$$

where l_i is the length of the projection of $\boldsymbol{b_i}$ onto the plane with $\boldsymbol{b}$ as the normal vector; m_i is the length of the projection of $\boldsymbol{b_i}$ onto the vector $\boldsymbol{b}$.

According to Eq.(10), we transform the objective function $\min ol(C)$ and have:

$$\min ol(C) \Leftrightarrow \max \sum_{i=1}^{k} m_i \Leftrightarrow \max \sum_{i=1}^{k} \langle \boldsymbol{b_i}, \boldsymbol{b} \rangle \tag{11}$$

$$\max \sum_{i=1}^{k} \langle \boldsymbol{b_i}, \boldsymbol{b} \rangle \Leftrightarrow \min \sum_{i=1}^{k} (\|\boldsymbol{b_i}\|^2 - 2\boldsymbol{b_i} \cdot \boldsymbol{b} + \|\boldsymbol{b}\|^2) \Leftrightarrow \min \sum_{i=1}^{k} \|\boldsymbol{b_i} - \boldsymbol{b}\|^2 \tag{12}$$

According to Eq.(11) and Eq.(12)，the objective function for the optimum build direction is:

$$\min \sum_{i=1}^{k} \|\boldsymbol{b_i} - \boldsymbol{b}\|^2 \tag{13}$$

The constraint condition is：

$$\|\boldsymbol{b}\|^2 = 1 \tag{14}$$

$$\|\boldsymbol{b_i}\|^2 = 1 \tag{15}$$

PCA [13] provides a solution for the problem of minimal 2-norm optimization. It converts the minimal optimization into the maximal optimization with $\max \boldsymbol{e}^T S \boldsymbol{e}$ as the objective function and $\boldsymbol{e}^T \boldsymbol{e} = 1$ as the constraint condition. By using Lagrange multiplier approach, we have $S\boldsymbol{e} = \lambda \boldsymbol{e}$. The eigenvector with the maximum eigenvalue for the sparse matrix S is our target. The sparse matrix S is estimated by the covariance matrix in the usage of PCA. When the number of points on the segment contour is few, there will be a greater estimation error between the sparse matrix and the covariance matrix. In this case, the confidence of the build direction will be reduced. Therefore, we must provide enough points to better estimate the sparse matrix. One efficient approach is the usage of high-precision input mesh.

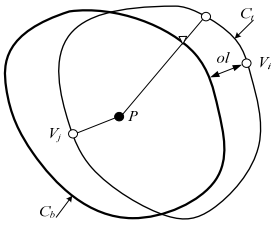

Fig.4 Overhang length between two adjacent layers

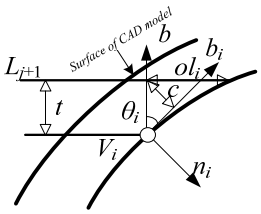

Fig.5 Overhang length and overhang angle for a single layer

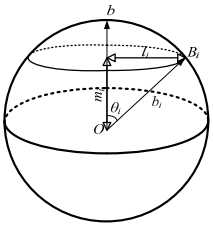

Fig.6 Gauss map of build directions

Segment thickness optimization

The segmentation consists of the initial segmentation and the overhang segmentation. For the former, the segment plane is parallel to the bottom of the AABB (Axis-aligned bounding box) of the input mesh and the segment thickness is the initial segment height. For the latter, the segment thickness is optimized to meet allowable overhang length and allowable cusp height. The concept of cusp height was proposed by Dolenc and Makela [14] and used to measure the stair-stepping error. For an overhang component, the cusp height also can be used to measure the missing

volume. As shown in Fig.5, there is a relationship between the cups height c and the segment thickness t, that is $t = \mathrm{c}/\sin(\theta)$. If θ tends to zero, the segment direction will tend to be coincided with the optimum build direction and t will tend to infinity. In this case, the segmentation will be failed. If θ approaches $\pi/2$, the segment direction will tend to be perpendicular to the optimum build direction and t will approach c. In this case, the segmentation will be also failed. To prevent the above exceptions, the segment thickness must be greater than or equal to the minimum segment thickness t_{min} and must be less than or equal to the maximum segment thickness t_{max}. Therefore, the segment thickness under allowable cups height is formulated by:

$$h_0 = \min\{t_1, t_2, \cdots t_k\} \tag{16}$$

$$h_0 \in [t_{min}, t_{max}] \tag{17}$$

Except for allowable cups height, the segment thickness must be constrained by allowable overhang length. Suppose that there is a linear relationship between the segment thickness and the overhang length. The actual overhang length can be calculated by Eq.(2), therefore the optimum segment thickness is:

$$h = \frac{ol_{max}}{ol_{calc}} h_0 \tag{18}$$

where ol_{max} is allowable overhang length corresponding to h_0 which is determined by slice thickness st and allowable overhang length sol_{max}. The detail relationship is:

$$ol_{max} = \frac{h_0}{st} sol_{max} \tag{19}$$

Examples and analyses

Fig.7 illustrates the details and results of the proposed algorithm used for the bend mesh. The corresponding input arguments are listed in Table 2. Fig.7*a* is the input mesh which has 5767 facets and 8652 edges. The dimension is $10.00 \times 23.17 \times 38.89$mm. Fig.7*b* illustrates the normal vector and the tangent vector for each point. Z-axis of each coordinate system is the optimal build direction for each segment mesh. Fig.7*c* illustrates the segment planes and the segment meshes. The bend is decomposed into eight segment meshes. Fig.7*d* illustrates the output slices. Except for the last segment mesh, each segment mesh has one segment contour and two slice contours. The last segment mesh only has one slice contour.

Fig.8 illustrates the overhang measurement comparison between the build direction unchanged and changed. The overhang measurement includes overhang length and overhang angle. The overhang angle and the overhang length for each point on the segment contour are calculated by Eq.(6) and Eq.(4). The allowable overhang length is 0.625mm which can be computed by Eq.(19). From Fig.8*a*, the overhang angle is significantly reduced and the maximum is reduced from 12.66° to 3.85°. From Fig.8*b*, the overhang length is reduced from 0.71mm to 0.60mm which less than 0.625mm. Therefore, both confirm feasibility and effectiveness of the proposed algorithm.

Table 2 Input arguments for Fig.7/mm

Allowable cusp height	c_{max}	-	Allowable overhang length	sol_{max}	.25
Maximum segment thickness	t_{max}	5	Minimum segment thickness	t_{min}	5
Initial segment height	*sh*	0	Slice thickness	*st*	2

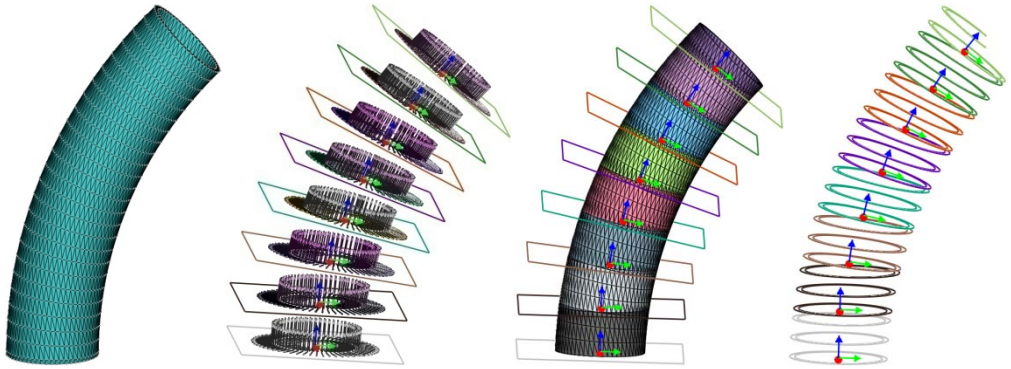

(a)input mesh; (b)normal and tangent vector; (c)segmented meshes; (d)output slices;
Fig.7 Adaptive slicing for the bend with uniform segment thickness

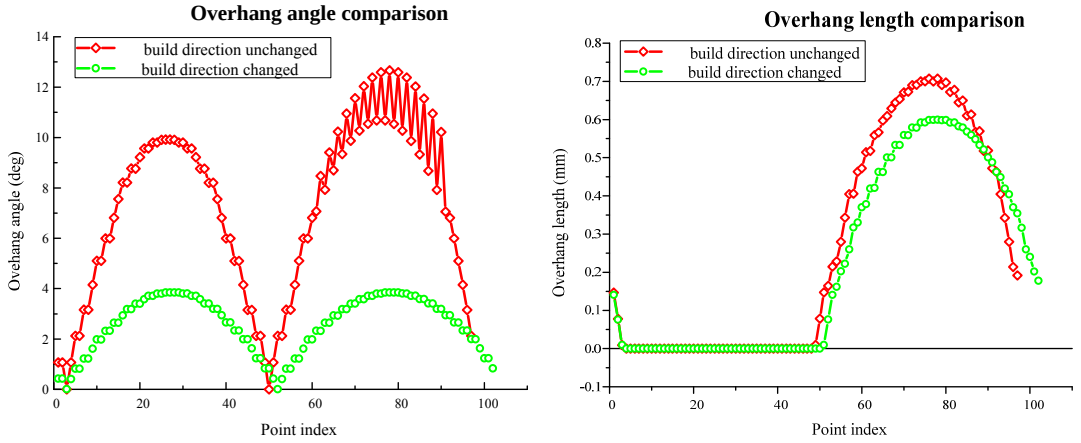

(a)overhang angle comparison; (b)overhang length comparison;
Fig.8 Overhang measurement comparison between build direction unchanged and changed

Different Fig.7, Fig.9 illustrates the segmentation with variable thickness. The corresponding input arguments are listed in Table 3. The bend is decomposed into six segment meshes. The segment thickness is small where the curvature is big and is big where the curvature is small. Fig.9*c* illustrates the adjustment of segment thickness. The pre-segment thickness, optimized thickness and actual thickness are computed by Eq.(16), (17) and (18) respectively. Build directions of the first segment mesh and the last segment mesh are parallel and their overhang lengths are less than the allowable value, therefore their segment thicknesses are the maximum allowable segment thickness. The thickness of the 2^{nd}-4^{th} segment meshes are less than the minimum allowable segment thickness. The thickness of the 5^{th} segment mesh is 5.43 which is between the minimum segment thickness and the maximum segment thickness. Fig.10 illustrates a more complex application example.

Table 3 Input arguments for Fig.9/mm

Allowable cusp height	c_{max}	1.2	Allowable overhang length	sol_{max}	.15
Maximum segment thickness	t_{max}	9	Minimum segment thickness	t_{min}	5
Initial segment height	*sh*	0	Slice thickness	*st*	1

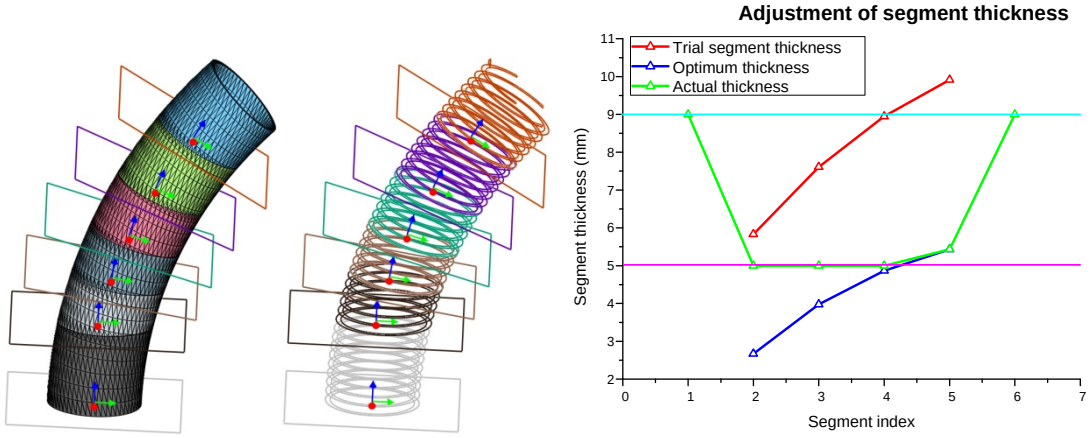

(a)segment meshes; (b)output slices; (c) adjustment of segment thickness

Fig.9 Adaptive slicing for the bend with variable segment thicknesses

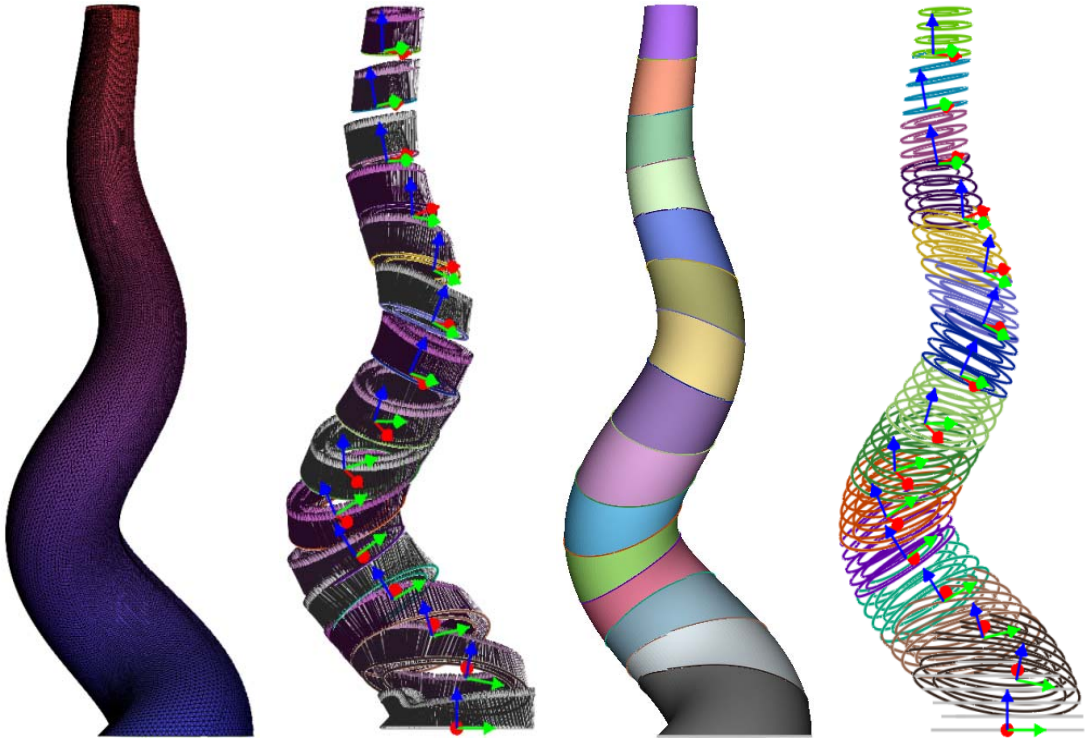

Fig.10 Adaptive slicing for the helix

Conclusions

To realize overhang component direct fabrication using multi-axis HPDM, an adaptive slicing algorithm with variable direction and thickness is proposed in this paper. It consists of multi-directional segmentation and single-directional slicing. The

former is applied to the input mesh to generate a series of non-uniform segment meshes, each of which can be fabricated directly without the usage of support. The latter is served for each sub-mesh to generate a series of slices, each of which with the same thickness is uniform. The segment direction is optimized to meet minimal overhang length and the segment thickness is adjusted to meet allowable overhang length and allowable cups height. The output slices consist of split slices between two adjacent segment meshes and inner slices for each segment mesh. The algorithm has been implemented by using C++ and OpenGL in the platform of VS2010. Examples and analyses confirm its feasibility and effectiveness.

Acknowledgement

We gratefully acknowledge the National Science Foundation of China (Grant Nos.51175203 and 51374113) for supporting this work.

References

1 Singh P, Dutta D. (2001). Multi-direction slicing for layered manufacturing. *Journal of Manufacturing Science and Engineering, Transactions of the ASME*, 123(2), pp.129-142.

2 Sundaram R K, Choi J. (2004). A slicing procedure for 5-axis laser aided DMD process. *Journal of Manufacturing Science and Engineering, Transactions of the ASME*, 126(3), pp.632-636.

3 Zhang J, Liou F. (2004). Adaptive slicing for a multi-axis laser aided manufacturing process. *Journal of Manufacturing Science and Engineering, Transactions of the ASME*, 126(2), pp.254-261.

4 Cornea N D, Silver D, Min P. (2007). Curve-skeleton properties, applications and algorithms. *IEEE Transactions on Visualization and Computer Graphics*, 13(2), pp.530-548.

5 Miklos B, Giesen J, Pauly M. (2010). Discrete scale axis representations for 3D geometry. *ACM Transactions on Graphics* (*TOG*), 29(4), pp.101.

6 Ruan J Z, Sparks T, Panackal A, *et al*. (2007). Automated slicing for a multi-axis metal deposition system. *Journal of Manufacturing Science and Engineering, Transactions of the ASME*, 129(2), pp.303-310.

7 Kabakabala D, Swathi R, Ruan J Z, *et al*. (2010) A multi-axis slicing method for direct laser deposition process. *Proceedings of the ASME Design Engineering Technical Conference, ASME*, pp.425-432.

8 Ren L, Sparks T, Ruan J Z, *et al*. (2008). Process planning strategies for solid freeform facrication of metal parts. *Journal of Manufacturing System*, 27(4), pp.158-165.

9 Zhang H O, Xu J P, Wang G L. (2002). Fundamental study on plasma deposition manufacturing. *Surface and Coatings Technology*, 171(1), pp.112-118.

10 Xiong X H, Zhang H O, Wang G L. (2008). A new method of direct metal prototyping: hybrid plasma deposition and milling. Rapid Prototyping Journal, 14(1), pp.53-56.

11 Xiong X H, Zhang H O, Wang G L. (2009). Metal direct prototyping by using hybrid plasma deposition and milling. *Journal of Materials Processing Technology*, 209(1), pp.124-130.
12 Makhanov S S. (2010). Adaptable geometric patterns for five-axis machining: a survey. *The International Journal of Advanced Manufacturing Technology*, 47(9-12), pp.1167-1208.
13 Jolliffe I T. Principal component analysis. Springer, 2002.
14 Dolenc A, Makela I. (1994). Slicing procedures for layered manufacturing techniques. *Computer-Aided Design*, 26(2), pp.119-126.